Journal Name

ARTICLE TYPE

Cite this: DOI: 00.0000/xxxxxxxxxx

Energy Transport in Glasses†

Elijah Flenner,*[a] Lijin Wang,*[b] and Grzegorz Szamel[a]

Received Date
Accepted Date

DOI: 00.0000/xxxxxxxxxx

The temperature dependence of the thermal conductivity is linked to the nature of the energy transport at a frequency ω, which is quantified by thermal diffusivity $d(\omega)$. Here we study $d(\omega)$ for a poorly annealed glass and a highly stable glass prepared using the swap Monte Carlo algorithm. To calculate $d(\omega)$, we excite wave packets and find that the energy moves diffusively for high frequencies up to a maximum frequency, beyond which the energy stays localized. At intermediate frequencies, we find a linear increase of the square of the width of the wave packet with time, which allows for a robust calculation of $d(\omega)$, but the wave packet is no longer well described by a Gaussian as for high frequencies. In this intermediate regime, there is a transition from a nearly frequency independent thermal diffusivity at high frequencies to $d(\omega) \sim \omega^{-4}$ at low frequencies. For low frequencies the sound waves are responsible for energy transport and the energy moves ballistically. The low frequency behavior can be predicted using sound attenuation coefficients.

The thermal conductivity of amorphous solids is vastly different than that of their crystalline counterparts. The existence of several common features in the temperature dependence of the thermal conductivity of amorphous solids indicates a common origin[1–8]. At temperatures below $\sim$ 1K the thermal conductivity grows as T^2 compared to T^3 growth for crystalline solids. This quadratic growth of the thermal conductivity with temperature is generally attributed to two-level tunneling states[3,5,7,9–11], although alternative explanations exist[12–14]. Around $T \approx 10K$ a plateau develops in the thermal conductivity and there is a nearly linear rise in the thermal conductivity after the plateau.

The temperature dependence of the thermal conductivity κ can be analyzed in terms of frequency dependent thermal diffusivity $d(\omega)$, which quantifies how fast a wave packet, narrowly peaked around a frequency ω, propagates[15–18]. At low temperatures, only the low frequency modes are excited, and only the low frequency thermal diffusivity significantly contributes to the thermal conductivity. The most prevalent theories attribute the low frequency thermal diffusivity to two-level states, which provide the dominant contribution below 1K, and to thermal transport due to sound waves[19,20]. By considering the sound waves as a phonon gas, Debye argued that there is a contribution to $d(\omega)$ given by $v(\omega)\ell(\omega)/3$ where $v(\omega)$ is the speed of sound and $\ell(\omega)$ is the mean free path[21]. It is often assumed, and confirmed in recent simulations, that sound attenuation obeys Rayleigh scaling, and thus the contribution due to sound waves behaves as $d_s(\omega) \sim \omega^{-4}$ [22–24]. Several researchers demonstrated that the thermal conductivity can be accurately described for temperatures at and below the low temperature plateau by combining the contributions to $d(\omega)$ due to two level systems and due to sound waves[19,20,25,26].

At room temperature, where all vibrational modes are excited, the average mean free path is on the order of the interatomic spacing[25,27–29], which implies that the high frequency excitations are strongly damped and can no longer be described as propagating sound waves. This strong damping is consistent with simulations, which show that energy transport does not have the low frequency ballistic character associated with sound waves[28,30,31]. Instead, for high frequencies the energy transport is diffusive. Xu *et al.*[17] showed that for systems of jammed spheres the thermal diffusivity is constant above a characteristic frequency ω_d up to a maximum frequency ω_c where it quickly drops to zero. The crossover frequency ω_d goes to zero as the unjamming transition is approached. This constant diffusivity can explain the linear increase of the thermal conductivity above the plateau. For high frequencies, the thermal diffusivity goes to zero and the excitations are localized[17,18,28,30,31].

Identification of these three regimes for $d(\omega)$ motivated Allen *et al.*[15,32] to characterize the vibrational modes in terms of propagons, diffusons, and locans. They determined that for amorphous silica 97% of modes are diffusons, which implies that diffusive transport is the dominant contribution to the thermal conductivity for temperatures above the plateau.

Few simulations have studied the full range of diffusivity from the low-frequency sound wave dominated regime to the high-

[a] *Chemistry Department, Colorado State University, Fort Collins, Colorado 80523, USA. E-mail: flennere@gmail.com*
[b] *School of Physics and Materials Science, Anhui University, Hefei 230601, P. R. China. E-mail: lijin.wang@ahu.edu.cn*

frequency plateau[28,30]. The method of Allen and Feldman[15,16] is currently restricted to high frequencies since one needs to diagonalize the Hessian, which restricts one to small systems. Here, we use an alternative method[28,30,31] to study the full range of frequencies, the crossover between high and low frequency, and the connection between the diffusivity and phonon attenuation. Additionally, to our knowledge, the energy diffusivity has not been studied as a function of the glass stability. Since the vibrational properties and the attenuation of sound waves change dramatically with stability[23,33,34], the energy diffusivity would also be expected to change with stability. Here, we compare the energy diffusivity over a broad range of frequencies for a poorly annealed glass and a glass whose stability is similar to that of stable laboratory glasses.

To calculate the thermal diffusivity we excite a narrow, in frequency and space, wave packet at the center of a simulation cell and examine energy transport in the harmonic approximation. For diffusive energy transport, the center of the wave packet remains stationary and the square of its width increases as $2d(\omega)t$ in each direction. We find that this method results in the same diffusivity as the method of Allen and Feldman[15,16] that uses the eigenvectors and eigenvalues of the Hessian. Since we excite a wave packet that can only propagate in one direction, we simulate elongated systems. These elongated systems allow us to extend the time scale for the energy transport calculation, and thus examine energy diffusivity at low frequencies where the transport is ballistic. Therefore, we can investigate the crossover from diffusive to ballistic energy transport.

1 Simulations

We create glasses by quenching a three-dimensional polydisperse model glass former equilibrated at a parent temperature T_p to its inherent structure using the fast inertia relaxation engine minimization algorithm[35]. The interaction between two particles n and m is given by

$$V(r_{nm}) = \varepsilon \left(\frac{\sigma_{nm}}{r_{nm}} \right)^{12} + v(r_{nm}) \qquad (1)$$

when $r_{nm} = |\mathbf{r}_n - \mathbf{r}_m| < 1.25\sigma_{nm}$ and zero otherwise. The continuity of $V(r_{nm})$ is ensured up to the second derivative at the cutoff by setting $v(r_{nm}) = c_o + c_2(r_{nm}/\sigma_{nm})^2 + c_4(r_{nm}/\sigma_{nm})^4$. The probability that a particle has a diameter σ is given by $P(\sigma) = A/\sigma^3$ where $\sigma \in [0.73, 1.63]$, and we use a non-additive mixing rule $\sigma_{nm} = 0.5(\sigma_n + \sigma_m)(1 - 0.2|\sigma_n - \sigma_m|)$. To equilibrate the systems at $T_p = 0.2$ and $T_p = 0.062$ we use the Monte Carlo swap algorithm[36,37]. The higher parent temperature is approximately equal to the onset temperature for the slow dynamics and the resulting inherent structure constitutes a poorly annealed glass. The lower parent temperature is lower than the estimated experimentally equivalent glass transition temperature of $T_g \approx 0.072$[37]. The inherent structure resulting from quenching the sample equilibrated at $T_p = 0.062$ constitutes a very stable glass. We present the results in reduced units where ε is the unit of energy and $\sqrt{M\sigma^2/\varepsilon}$ is the unit of time. Each particle has the same mass M, which is our mass unit. We set Boltzmann constant $k_B = 1$.

We equilibrated systems of $N = 3000$ and $N = 48000$ particles at a number density $\rho = N/V = 1.0$. Since at low frequencies the energy moves ballistically at the speed of sound, we needed large systems. To this end we replicated the $N = 3000$ particle system 80 times in the x-direction to make a very elongated simulation box with 243000 particles. We replicated the 48000 particle system two times to make a 144000 particle system. We have checked that there were no finite size effects.

To study the energy transport we excited a wave-packet centered at $x = 0$. To this end we solved the harmonic equations of motion

$$\ddot{\mathbf{u}}_n(t) = -\sum_{n=1}^{N} \mathbf{D}_{nm} \cdot \mathbf{u}_m(t) + \mathbf{f}_n(\phi, \omega, x, t), \qquad (2)$$

where $\mathbf{u}_n = \mathbf{r}_n - \mathbf{r}_n^0$, $\mathbf{r}_n^0$ is the inherent structure position, $\mathbf{D}_{nm}$ is the dynamical matrix (Hessian). The external force exciting the wave packet, $\mathbf{f}_n(\phi, \omega, x, t)$, is given by

$$\begin{aligned} \mathbf{f}_n(\phi, \omega, x, t) &= \mathbf{a}_\lambda \cos(\omega t + \phi) \\ &\quad \times \exp\left[-\frac{1}{2}\left(\frac{x}{\Delta x}\right)^2 - \frac{1}{2}\left(\frac{t}{\Delta t}\right)^2 \right]. \end{aligned} \qquad (3)$$

We started the simulation at $t = -5\Delta t$ so that $\mathbf{f}_n(\phi, \omega, x, t) \approx 0$ and run until the excitation reaches the end of the simulation box. Unless otherwise noted, we use $\Delta x = 0.5$ and $\Delta t = 10$. Since a wave-packet of finite duration is a mixture of different frequencies, our frequency uncertainty is $\Delta\omega \approx 1/(\Delta t) = 0.1$.

2 Energy Transport Calculation

We use an approach proposed by Beltukov *et al.*[28] and run two simultaneous simulations using the same system. The simulations differ by the phase ϕ in the external force exciting the wave packet. For the first simulation $\phi = 0$ and for the second simulation $\phi = \pi/2$. Alternatively, one can run one simulation and divide the kinetic and potential energy into regions, but it is ambiguous how to divide the potential energy between the two interacting particles. Beltukov *et al.*'s approach removes that ambiguity.

The energy is converted from potential to kinetic at a rate given by ω and the energy density can be defined as

$$E(\omega, x, t) = \frac{1}{2 l_y l_z} \sum_n \left[(\dot{\mathbf{u}}_n^0)^2 + (\dot{\mathbf{u}}_n^{\pi/2})^2 \right] \delta(x - x_n), \qquad (4)$$

where $\dot{\mathbf{u}}_n^\phi$ is the velocity of particle n in simulation with phase ϕ at a time t, l_y is the box length in the y direction, and l_z is the box length in the z direction. We study longitudinal excitations by setting $\mathbf{a}_L = (a, 0, 0)$ and transverse excitations by setting $\mathbf{a}_T = (0, 0, a)$. We also study random excitations that are described by $\mathbf{a}_T = (a r_x, a r_y, a r_z)$ where r_x, r_y, and r_z are Gaussian distributed random numbers of unit variance. Since we are using the harmonic approximation, the results are independent of the value of a. If energy transport is diffusive, the thermal diffusivity $d(\omega)$ can be calculated by calculating $\delta r^2(\omega, t) = \int dx x^2 E(\omega, x, t) / \int dx E(\omega, x, t)$ and fitting $\delta r^2(\omega, t) = 2d(\omega)t + r_0^2$ for the range of times when $\delta r^2(\omega, t)$ is linear. If the energy transport is ballistic, then $\delta r^2(t) \sim t^2$.

An alternative approach to determine the thermal diffusivity is

due to Allen and Feldman [15,16]. This approach was used in several simulations utilizing the harmonic approximation [17,18,28,30]. Within Allen and Feldman's approach, the thermal diffusivity is determined from the eigenvalues and eigenvectors of the Hessian matrix. This approach is time consuming and suffers from finite size effects [33,38]. We used the method of Allen and Feldman and compared the resulting thermal diffusivity with the thermal diffusivity obtained from Beltukov *et al.*'s approach.

According to Allen and Feldman's approach, the thermal diffusivity can be calculated as follows

$$d_{AF}(\omega) = \frac{\pi}{12M^2\omega^2}\int_0^\infty d\omega' D(\omega') \times \frac{(\omega+\omega')^2}{4\omega\omega'}\left|\mathbf{S}(\omega,\omega')\right|^2\delta(\omega-\omega'). \quad (5)$$

The heat-flux matrix elements are given by

$$\left|\mathbf{S}(\omega,\omega')\right|^2 = \frac{\sum_{mn}|\mathbf{S}_{nm}|^2\,\delta(\omega-\omega_m)\delta(\omega'-\omega_n)}{D(\omega)D(\omega')}, \quad (6)$$

where the sum is over the vibrational modes. The matrix elements $\mathbf{S}_{mn}$ are

$$\mathbf{S}_{mn} = \sum_{i,j}(\mathbf{r}_i - \mathbf{r}_j)\mathbf{e}_{m,i}\cdot\mathbf{D}_{i,j}\cdot\mathbf{e}_{n,j}, \quad (7)$$

where $\mathbf{e}_{n,i}$ is the normalized eigenvector of the Hessian matrix. For a finite system the delta function in equation 5 is replaced by $g(\omega_m-\omega_n,\eta) = \eta/\{\pi[(\omega_m-\omega_n)^2+\eta^2]\}$ where we have set $\eta = 0.01$.

3 Thermal Conductivity

The thermal conductivity κ can be expressed in terms of $d(\omega)$, the density of states $D(\omega) = \sum_m \delta(\omega-\omega_m)$ and the heat capacity $C(\omega,T)$ using the following formula [16,31,39]

$$\kappa = \frac{1}{V}\int_0^\infty d\omega D(\omega)d(\omega)C(\omega,T). \quad (8)$$

The heat capacity $C(\omega,T) = k_B(\beta\hbar\omega)^2 e^{\beta\hbar\omega}/(e^{\beta\hbar\omega}-1)^2$, where $\beta = 1/k_BT$, T is the temperature, and $\hbar$ is the reduced Planck constant.

Although according to the standard nomenclature $d(\omega)$ is referred to as the energy diffusivity, the energy transport does not have to be diffusive, and it can arise from other mechanisms. Here we calculate $d(\omega)$ within the classical harmonic approximation, and thus we ignore anharmonic effects that are important to understanding the full temperature dependence of $d(\omega)$. The most important neglected effect is proposed to be scattering due to two-level systems that is both quantum mechanical and anharmonic [3,5,7]. Our approach marks a starting point and quantum mechanical and anharmonic effects are left for future work.

When there is more than one energy transport mechanism, it is usually assumed that $d^{-1}(\omega) = \sum_n d_n^{-1}(\omega)$ where $d_n(\omega)$ correspond to different energy transport mechanisms [19,20,25,26]. At low frequencies, the dominant energy transport mechanism is sound waves (in the harmonic approximation) and $d^{-1}(\omega) \approx d_L^{-1}(\omega) + d_T^{-1}(\omega)$ where $d_L(\omega)$ is the contribution due to longitudinal sound waves and $d_T^{-1}(\omega)$ is due to the transverse waves. It is expected that the energy transport is dominated by the transverse waves, and $d(\omega) \approx d_T(\omega)$. By exciting longitudinal and transverse wave packets we examine individually the energy transport due to longitudinal sound waves and transverse sound waves. Additionally, the random wave packet allows us to examine how the energy transport separates into contributions from longitudinal and transverse waves, and we can determine the dominant energy transport mechanism.

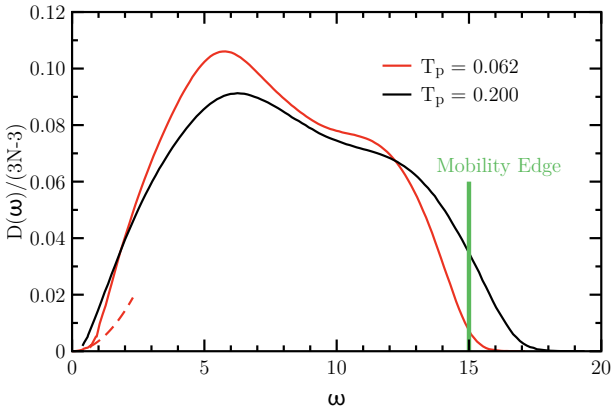

Fig. 1 Normalized density of states for a stable glass $T_p = 0.062$ (red line) and for a poorly annealed glass $T_p = 0.2$ (black line). The dashed red line is the Debye prediction for the density of states for $T_p = 0.062$. The green line marks the mobility edge, where the energy remains localized and does not propagate.

4 Density of States

Before we discuss the temperature and stability dependence of the thermal conductivity, we first examine the density of states. Shown in Fig. 1 is the density of states $D(\omega)/(3N-3)$ normalized so that its integral over all frequencies is equal to one, and thus does not depend on the system size. We show the density of states for a stable glass with parent temperature $T_p = 0.062$ (red line) and a poorly annealed glass with $T_p = 0.2$ (black line). The dashed red line is the Debye density of states $3\omega^2/\omega_D^3$ for $T_p = 0.062$, where Debye frequency $\omega_D = [(18\pi^2\rho)/(v_L^{-3}+2v_T^{-3})]^{1/3}$, v_L is the longitudinal speed of sound, and v_T is the transverse speed of sound. The speed of sound was obtained from our previous work on sound attenuation [23]. The excess modes above the Debye prediction for the low-frequency modes are clearly visible. In previous works, it was shown that the low frequency density of states can be divided into contributions due to extended and quasi-localized modes [22,23,40]. The density of states of the extended modes agrees with the Debye prediction, while the density of states of the low-frequency localized modes scales as ω^4. This scaling of the localized modes has been observed in several simulational studies [22,23,40–43] and predicted using different theoretical arguments [19,44–50].

The more stable glass has fewer low frequency modes, which can be attributed to an increase in ω_D ($\omega_D = 9.43$ for $T_p = 0.062$ and $\omega_D = 8.39$ for $T_p = 0.2$), which is mainly driven by an increase in the shear modulus (the transverse sound speed). However, there is also a decrease in the number of quasi-localized modes [23].

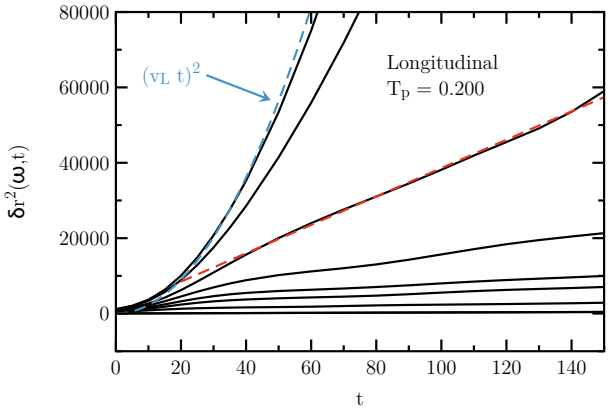

Fig. 2 Mean squared width of the wave-packet $\delta r^2(\omega,t)$ for $\omega = 0.3$, 0.4, 0.6, 0.8, 1.0, 1.2, 1.4, 5.0, and 10.0 listed from top to bottom. The red dashed line is a fit to $\omega = 0.6$ for $t \geq 50$. The blue dashed line is $[v_L(\omega)t]^2$ for $\omega = 0.3$.

The poorly annealed glass has more modes in the high frequency regime, above $\omega \approx 13$. The contribution of these modes to the thermal conductivity will depend on whether the modes are diffusive or localized, since the localized modes do not contribute to the thermal conductivity in the harmonic approximation. For frequencies between $\omega \approx 1.7$ and $\omega \approx 12.3$ the density of states is greater for the stable glass.

5 Energy Transport

Here we will examine the energy transport that follows exciting a longitudinal wave packet, a transverse wave packet, and a random wave packet. At low frequencies, after exciting the longitudinal wave packet the energy moves *via* longitudinal sound waves and after exciting the transverse wave packet the energy moves *via* transverse sound waves. At high frequencies, when the energy transport is diffusive, the two excitations produce the same results. However, the situation is different for the random wave packet. Here we will find that at low frequencies the energy transport divides itself into a longitudinal and transverse contribution that travel ballistically at the speed of longitudinal and transverse sound, respectively.

In Fig. 2 we show examples of the time dependence of the mean square width of the wave packet, $\delta r^2(\omega,t)$, for $T_p = 0.2$ for $\omega = 0.3$, 0.4, 0.6, 0.8, 1.0, 1.2, 1.4, 5.0, and 10.0 listed from top to bottom. The external force starts at $t = -50$, reaches its maximum at $t = 0$ and is effectively zero by $t = 50$. If the energy transport is diffusive, we can fit $\delta r^2(\omega,t) = 2d(\omega)t + a$ to obtain the diffusivity $d(\omega)$. We show such a fit to $\omega = 0.6$ as a red dashed line. Once the sound waves are the main carriers of the energy, then the energy transport is ballistic and $\delta r^2(\omega,t) = (v_L(\omega)t)^2$, which is shown as the blue dashed line. The longitudinal speed of sound $v_L(\omega)$ was obtained from previous work on sound attenuation[33]. We observe that the calculated $\delta r^2(\omega,t)$ nearly matches this prediction for $\omega = 0.3$, but we cannot rule out an eventual linear increase for times inaccessible in our simulations.

In Fig. 3 we present the thermal diffusivity $d(\omega)$ calculated for longitudinal (red squares), transverse (blue circles), and random (black triangles) excitations for a poorly annealed glass, $T_p = 2.0$ (a), and a stable glass, $T_p = 0.062$ (b). At high frequencies, $\omega > 15$, the energy stays localized. This limit is denoted as the mobility edge in Fig. 3 and Fig. 1. The mobility edge is not sensitive to the glass's stability. However, as seen in Fig. 1 there are many more vibrational modes above the mobility edge for the poorly annealed glass than for the stable glass.

With decreasing frequency, the diffusivity increases between $\omega \approx 15$ and $\omega \approx 10$. Between $\omega \approx 10$ and $\omega \approx 2$ the diffusivity is nearly constant and independent of the nature of the excitation. As can be seen from Fig. 1, there are more modes within the plateau of the diffusivity for the stable glass than for the poorly annealed glass. We also show the diffusivity calculated using the method of Allen and Feldman[15,16] $d_{AF}(\omega)$ (dashed green line) for $T_p = 0.062$ and find excellent agreement within the plateau region, which verifies the physical picture of d_{AF}. Due to the small size of the simulation box, it is not possible to obtain diffusivity at small ω using the method of Allen and Feldman. Additionally, it has been recently observed that there are finite size effects in calculations of vibrational modes from the Hessian matrix[33,34,38], which may result in calculated thermal diffusivity $d_{AF}(\omega)$ that does not correspond to the thermodynamic limit.

Below $\omega \approx 2$ the diffusivity rapidly increases with decreasing ω for each type of excitation. The departure from the plateau is independent of the glass's stability. Therefore, the contribution to the thermal conductivity due to the plateau region is due to the difference in the density of states and not due to the thermal diffusivity, since the thermal diffusivity is stability independent over this region. The longitudinal diffusivity increases faster with decreasing ω than both the transverse and the random excitation. For low frequencies and our most stable glass, both the longitudinal and the transverse diffusivities appear to increase as ω^{-4} as shown by the red and blue lines in Fig. 3.

For our poorly annealed glass, we fit $d(\omega)$ for the longitudinal excitation for $\omega < 1.5$ to $d(\omega) = B\omega^{-4}$, which is shown as the red dashed line in Fig. 3. We note that for $\omega > 0.6$ we clearly observe a linear increase of $\delta r^2(\omega,t)$ with time t, as shown in Fig. 2. This linear time dependence is expected for diffusive energy transport, but in Section 6 we will see that for a range of frequencies the energy density is not well described by a Gaussian distribution indicative of diffusive energy transport. We note that the data for transverse diffusivity do not follow ω^{-4} scaling in the frequency range that we could examine but we expect that $d(\omega) \sim \omega^{-4}$ at lower frequencies, in agreement with the stable glass.

We now show that the frequency dependence of $d(\omega)$ is consistent with $d(\omega) = v_L\ell(\omega)/3$ where the mean free path $\ell(\omega) = v_L/\Gamma_L(\omega)$ and $\Gamma_L(\omega)$ is the sound attenuation coefficient. In earlier work we found that transverse sound attenuation $\Gamma_T(\omega)$ could be rescaled by a constant factor so that it overlaps with longitudinal sound attenuation $\Gamma_L(\omega)$[33]. In the inset to Fig. 3(a) we show this rescaling and the dashed line shows $\Gamma_L(\omega) = [v_L^2/(3B)]\omega^4$ where B is obtained from the fit to $d(\omega)$ shown in the main plot in Fig. 3(a). The scaling of $d(\omega)$ smoothly continues into the propagating regime where it is no longer appropriate to consider the energy transport as diffusive.

In the previous paragraph we showed the the low frequency

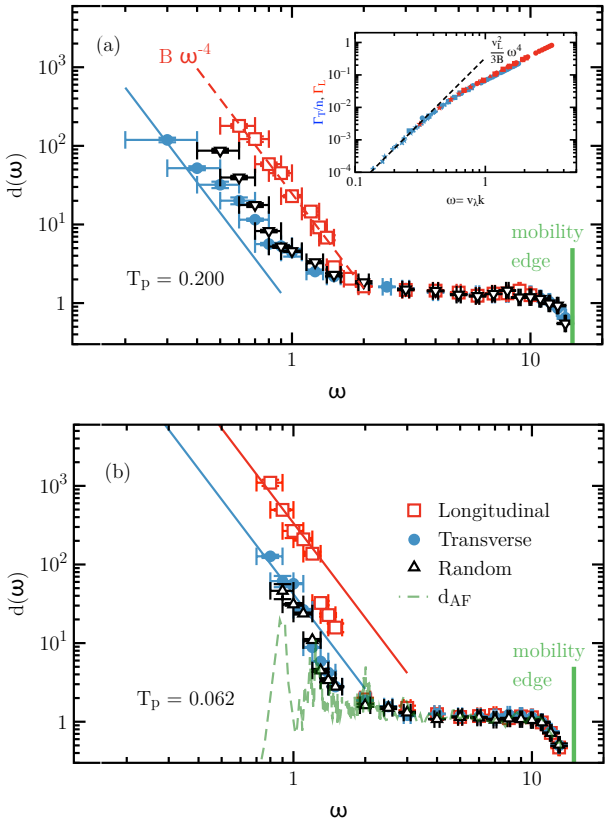

Fig. 3 Energy diffusivity for $T_p = 0.2$ (a) and $T_p = 0.062$ (b). The red squares are results for the longitudinal excitation, the blue circles are results for the transverse excitation, and the black triangles are results for the random excitation. The dashed red line in (a) is a fit to $d(\omega) = B\omega^{-4}$. We use the phonon gas model and calculations of sound attenuation to predict $d(\omega)$ at low frequencies, and these predictions are given by the solid blue (transverse) and red (longitudinal) lines.

behavior of thermal diffusivity calculated for the longitudinal excitation can be used to reproduce the low frequency behavior of the sound attenuation. Now, we will show that the opposite can also be done. To this end we used the low frequency behavior of $\Gamma_\lambda(\omega)$ for longitudinal sound waves ($\lambda = L$) and for transverse sound waves ($\lambda = T$) obtained from previous work[33] to predict the low frequency behavior of $d(\omega)$. The results are shown as solid lines in Fig. 3(a) and (b). From the low frequency behavior $\Gamma_\lambda(\omega) = A_\lambda \omega^4$ we predict that the thermal diffusivity should be given by $v_L^2/(3A_L\omega^4)$ and $2v_T^2/(3A_T\omega^4)$, for the longitudinal and transverse excitation, respectively. The factor of 2 for the transverse excitation is due to the two polarizations. The red line illustrates the predicted behavior of the thermal diffusivity for the longitudinal excitation and the blue lines show the predicted behavior of the thermal diffusivity for the transverse excitation. We observe this smooth continuation of the diffusivity from diffusive energy transport to ballistic energy transport with decreasing frequency for each type of excitation.

It is natural to assume that $d(\omega) = v\ell(\omega)/3$ up until the sound waves are no longer well defined, which is generally associated with the Ioffe-Regel limit. We determined the Ioffe-Regel limit for this system for both the longitudinal and transverse sound waves. The Ioffe-Regel limit ω_{IR} for transverse sound, which is lower than for longitudinal sound, for $T_p = 0.062$ is $\omega_{IR} = 1.74$ and for $T_p = 0.200$ it is $\omega_{IR} = 0.9$. The ω^{-4} scaling does not extend to these frequencies for the transverse sound waves for either parent temperature, and thus the Ioffe-Regel criteria does not determine the cutoff for the ω^{-4} energy transport. However, it does give an upper bound.

For most frequencies the random excitation follows the transverse excitation, but we observe statistically significant deviations from this behavior for $T_p = 0.200$ at the smaller frequencies. To get some insight into these deviations, in the next section we will examine in detail the time dependence of the energy density.

6 Energy Density

The physical interpretation of the energy diffusivity $d(\omega)$ proposed by by Allen and Feldman[15,16] is based on the thought experiment that considers the time evolution of a wave packet narrowly peaked at ω and initially spatially localized. The square of the width of the wave packet at a time t divided by $2t$ is $d(\omega)$[16]. This is the operational definition we used in Section 5. However, the wave packet does not always propagate diffusively and for low frequencies the square of the width increases as t^2. In this section we examine time dependent energy density $E(\omega,x,t)$ for a random excitation. We compare this energy density with those resulting from the transverse and longitudinal excitations. In this way we clarify the role of sound waves in the energy transport. We find that diffusive energy transport describes the excitation in the plateau region, and very clear wave packets propagating at a constant velocity emerge for low frequency excitations. However, at intermediate frequencies the wave packets are no longer well described as diffusive or propagating. Similar sort of behavior has been observed in simulations of amorphous silicon[28,30].

We begin by examining $E(\omega,x,t)$ for the random excitation at $\omega = 4$, which is shown in Fig. 4 for $t = 50$ (black circles), 150 (blue triangles), and 250 (green squares). We also show Gaussian fits to the energy density, $E(\omega,x,t) \sim \exp[-x^2/(4d_{\rm fit}t)]$ (solid lines), which describe $E(\omega,x,t)$ well. We find that $d_{\rm fit} \approx 1.1$ agrees well with the value of 1.08 we found by fitting $\delta r^2(\omega,t)$. There is some ambiguity as to when to define $t = 0$ for the wave packet, which effects the value of $d_{\rm fit}$. Here it is defined as the time when the force is the largest.

At low frequencies, the time dependence of the wave packet for a random excitation is very different from that at high frequencies. Shown in Fig. 5 are results for $\omega = 0.5$ for $T_p = 0.062$ for $t = 50$ (black), 70 (red), 90 (blue), and 110 (green). The wave packet breaks up into two parts, where one corresponds to energy transport due to longitudinal sound waves and the other corresponds to energy transport due to transverse sound waves. The longitudinal sound waves travel faster, and thus the longitudinal part separates from the transverse part and two clear wave packets emerge. For $t = 110$ we can see where the longitudinal wave packet crosses the boundary of the simulation box and interacts with itself. To confirm this interpretation of the two wave packets, we verified that the center of the transverse and longitudinal

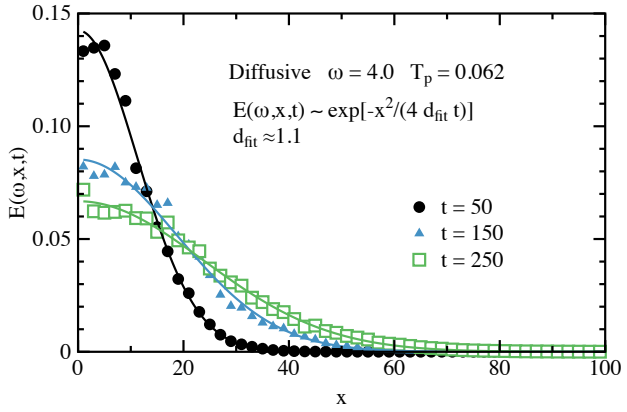

Fig. 4 The energy density for a random excitation for the most stable glass, $T_p = 0.062$, at $\omega = 4.0$. The solid lines are fits to diffusive energy transport.

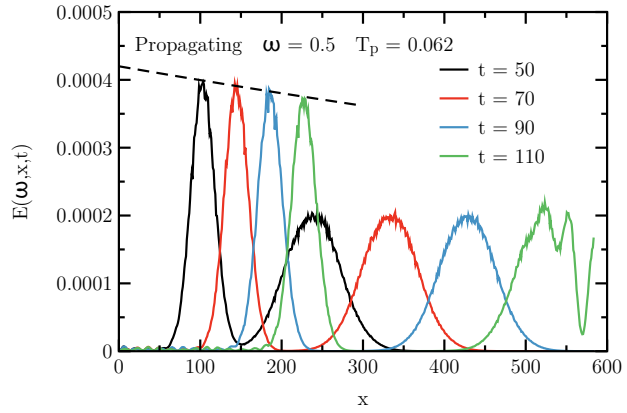

Fig. 5 The energy density for a random excitation for the most stable glass, $T_p = 0.062$, at $\omega = 0.5$. The energy breaks up into a propagating transverse wave packet and a propagating longitudinal wave packet.

wave packet moves at a velocity $v_T(\omega)$ and $v_L(\omega)$, respectively.

The mean free path of the transverse excitation $\ell(\omega)$ is given by $\ell(\omega) = 3d(\omega)/v_T(\omega)$, and the relationship between $d(\omega)$ and sound attenuation $\Gamma(\omega)$ was discussed in Section 5. In previous work we demonstrated that $\Gamma(k) = B_T k^4$ for small k, and thus $\ell(\omega) = 2v_T^6/(B_T\omega^4)$ assuming a linear dispersion relation $\omega = v_T k$. For $\omega = 0.5$ we use our fit to $\Gamma(k)$ from the previous work[33] and obtain $\ell(0.5) \approx 2011$. Shown as a dashed line in Fig. 5 is $a\exp[-x/\ell(0.5)]$, and we find that from the low frequency (small wavevector) sound attenuation one can predict the decay of the envelope of the transverse wave packet. To determine $\ell(\omega)$ from the decay of the envelope of the wave packet is difficult due to small decay over the available time range, but is conceptually possible.

For ω between the pure diffusive regime and the pure ballistic regime the energy density has a very different time dependence. Shown in Fig. 6 is $E(\omega,x,t)$ for $\omega = 0.6$, $T_p = 0.2$ at the time $t = 50$ (black), 100 (red), 150 (blue) and 200 (green). Here we do not observe a Gaussian distribution of the energy density at any time, and there exists a long tail in the energy density. However, the width characterized by $\delta r^2(\omega,t)$ grows linearly, which is shown

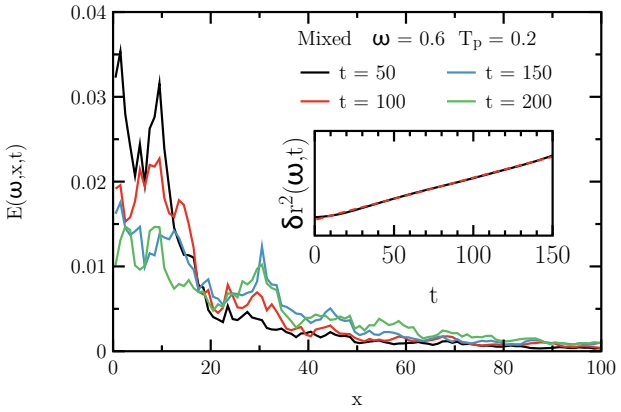

Fig. 6 The energy density for a random excitation for a poorly annealed glass, $T_p = 0.2$, at $\omega = 0.6$. The inset shows that $\delta r^2(\omega;t)$ is linear, but the main figure demonstrates that the energy density is not Gaussian.

in the inset. This linear growth allows us to calculate $d(\omega)$ for $\delta r^2(\omega,t)$.

Energy transport does not begin to become ballistic for both the longitudinal and transverse waves for the same frequency for our poorly annealed glass. This difference in the energy transport of a longitudinal and transverse excitation for $\omega = 0.3$ and $T_p = 0.2$ is shown in Fig. 7. Here we observe two different types of behavior. By comparing with the longitudinal excitation, we find that there is a propagating wave packet that is proportional to the longitudinal excitation. The propagating part moves at a constant velocity that is equal to the velocity of the longitudinal sound wave. The other contribution to the energy density behaves much like the transverse excitation for this frequency and parent temperature.

The energy transport at $\omega = 0.3$ and $T_p = 0.2$ is carried by a longitudinal sound wave but not by a transverse sound wave. Therefore, at least for our poorly annealed glass, there is a narrow frequency window where longitudinal sound waves significantly contributes to the energy transport, but transverse sound waves do not. For low frequencies, the energy transport will be dominated by the transverse sound waves. We never observed a similar scenario for the stable glass, $T_p = 0.062$, but cannot rule out that one exists over a narrow frequency range. This difference in the frequency at which energy transport is dominated by the sound waves for longitudinal and transverse sound results in the difference between $d(\omega)$ given by a random excitation and the transverse excitation in Fig. 3(a).

7 Discussion and Conclusions

We found that the frequency dependence of the thermal diffusivity in glasses, as calculated within the harmonic approximation, can be divided into four main regions. For low ω energy transport is dominated by transverse sound waves whose attenuation Γ obeys a Rayleigh scattering law[24,33]. Therefore, at low frequencies $d(\omega) = A_{\rm low}\omega^{-4}$ where $A_{\rm low}$ can be predicted from the attenuation of transverse sound waves. There is an intermediate regime where the longitudinal sound waves dominate the energy transport, but this regime may be very narrow or not exist for well annealed glasses. At high frequencies the diffusivity is

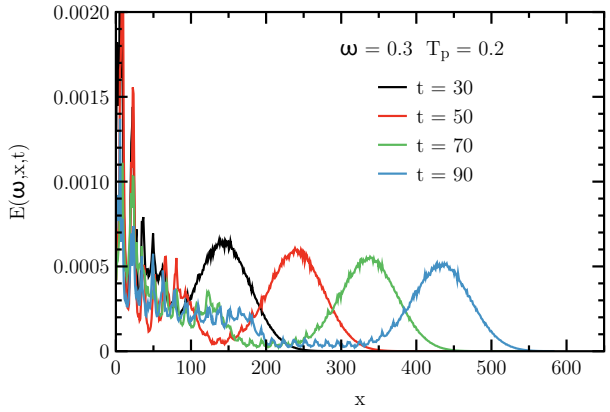

Fig. 7 The energy density for a random excitation for a poorly annealed glass, $T_p = 0.2$, at $\omega = 0.3$. We find that the wave packet can be separated into components that are proportional to a transverse excitation and a longitudinal excitation. The longitudinal component moves at the constant speed of a longitudinal wave for $\omega = 0.3$.

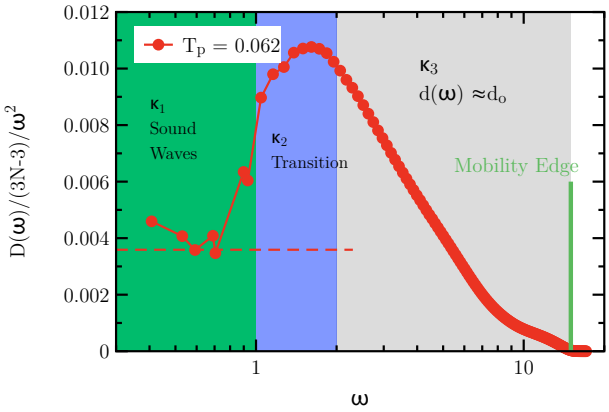

Fig. 8 The reduced density of states for $T_p = 0.062$ with different regions of energy transport highlighted. The green region indicates the frequencies where sound waves dominate the energy transport, and the gray region is the region of nearly constant diffusivity. The blue region indicates the transition region between the two.

nearly flat up to a cutoff frequency ω_m. The transition between the flat diffusivity and the asymptotic ω^{-4} scaling occurs over a range $\omega_1 < \omega < \omega_2$ where ω_1 is stability dependent but ω_2 only weakly depends on stability if at all. We find that the Ioffe-Regel frequency is within that window, but does not mark the upper end or the lower end of the frequencies. The lower end of the transition region, ω_1, is stability dependent, but the upper end ω_2 is independent of the stability.

These observations lead to breaking the harmonic approximation to the thermal conductivity into three main contributions $\kappa \approx \kappa_1 + \kappa_2 + \kappa_3$ where κ_1 is the contribution from sound waves, κ_2 is the contribution from the transition region, and κ_3 is the contribution from the nearly constant region of diffusivity. Shown in Fig. 8 is the reduced density of states $D(\omega)/(3N-3)/\omega^2$ for $T_p = 0.062$ with three regions highlighted. For $\omega < 1.0$ sound waves are predominantly responsible for energy transport, and this is indicated by the green region. For $1.0 < \omega < 2.0$ there is a change to a nearly flat $d(\omega) \approx d_0$, and this transition region is highlighted light blue. For $\omega > 2.0$ the diffusivity $d(\omega) \approx d_o$ is nearly constant up until the mobility edge at $\omega \approx 15$. The region of nearly constant $d(\omega)$ is highlighted gray.

At low temperatures the κ_1 term would dominate due to the weight $C(\omega, T)$. It has been established that the low frequency density of states can be divided into two parts. One part is due to extended modes, which obey Debye scaling, and one part is due to low-frequency, quasi-localized modes[23,40]. For these low frequencies, $D(\omega)/(3N-3) = 3\omega^2/\omega_D^3 + A_4\omega^4$. The value of A_4 represents the contribution to the density of states from the quasi-localized modes, and thus is not the main contribution to the energy transport. Neglecting the contribution due to the quasi-localized modes we can write κ_1 as

$$\kappa_1 \approx \frac{6\rho\hbar v_T^2}{\omega_D^3 B_T}\frac{1}{T}\int_0^{x_1} dx \frac{e^x}{(e^x-1)^2}, \tag{9}$$

where $x = \hbar\omega/(k_B T)$ and B_T is the coefficient that describes sound attenuation $\Gamma(\omega)$, $\Gamma(\omega) = B_T\omega^4$. The integral diverges due to the $x = 0$ limit. This divergence can be avoided by setting a lower limit to the integration at $\omega_{\min} = v_T 2\pi/L$ where L is the length of the amorphous solid or the divergence can be avoided by including anharmonic contributions. Two level states are the most likely candidate for the low frequency anharmonic contribution. We note that $\kappa_1 \sim 1/T$ and would result in a leveling off of the T^2 contribution that arises from two level states with increasing temperature.

The second contribution κ_2 represents the transition between the low frequency ω^4 contribution to $d(\omega)$ and the nearly flat diffusivity at higher ω. For our poorly annealed glass there is a range of ω where there is a significant contribution to $d(\omega)$ due to longitudinal sound waves, but no contribution due to transverse sound waves. We do not see this behavior for our stable glass and $d(\omega)$ drops below the extension of the asymptotic small ω sound wave result. This intermediate regime extends over a limited range and deserves more study. We determined the frequency of the boson peak $\omega_{BP} = 1.63$ for $T_p = 0.062$ and $\omega_{BP} = 0.713$ for $T_p = 0.2$, which is in this transition region of $d(\omega)$.

The third contribution κ_3 is due to the region of approximately flat diffusivity. If we assume that $d(\omega) \approx d_0$, then

$$\kappa_3 \approx 3\rho d_0 \int_{\omega_2}^{\omega_m} d\omega D(\omega) k_B \left(\frac{\hbar\omega}{k_B T}\right)^2 \frac{e^{\hbar\omega/(k_B T)}}{(e^{\hbar\omega/(k_B T)}-1)^2}. \tag{10}$$

In the inset to Fig. 9 we show this integration range as the shaded area under the density of states for $T_p = 0.062$. Most of the vibrational modes are within this region, with 94% of the vibrational density of states within this region for $T_p = 0.2$ and 97% within this region for $T_p = 0.062$. Unlike upon the approach to the unjamming transition[17], the density of states does not demonstrate any regions where both the diffusivity and the density of states are nearly flat. To check the temperature dependence of this contribution, we numerically integrate κ_3 assuming that $d(\omega) = d_0 = 1.15$ and set $\hbar$ and k_B to one.

Shown in Fig. 9 is κ_3 versus temperature for the stable glass $T_p = 0.062$ (solid line) and the poorly annealed glass $T_p = 0.2$

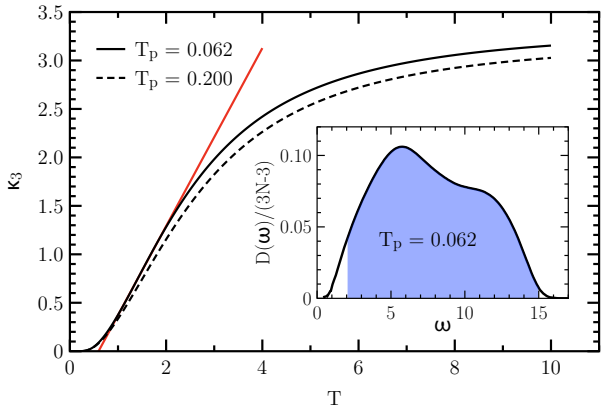

Fig. 9 The contribution to the thermal conductivity due to the region of nearly constant diffusivity, κ_3. The red line is a fit to κ_3 between $T = 1$ and $T = 2$. (inset) The vibrational density of states for $T_p = 0.062$ with the shaded region showing the range of ω of approximate constant diffusivity.

(dashed line). This contribution to the thermal conductivity is what is observed for amorphous solids above the $T \approx 10K$ plateau. For low temperatures κ_3 is negligible, which corresponds to temperatures at and below the plateau in the thermal conductivity. For temperatures above the plateau, and the vibrational states above ω_2 become populated, there is a near linear increase of κ_3. The red line is a linear fit to κ_3 for $1 \leq T \leq 3$ for $T_p = 0.062$. At high temperatures, $C(\omega, T) \approx k_B$ and κ_3 saturates. As suggested by studies[17] of systems approaching the unjamming transition, the region of flat diffusivity can accurately describe the behavior of the thermal conductivity above the plateau at approximately $10K$.

We find that the main difference between energy transport in the two systems is at low frequencies where sound waves are the dominate contribution. With increasing stability, sound attenuation decreases[33] resulting in an increase in $d(\omega)$. The decreased sound attenuation is also accompanied by a decrease in the number and spatial extent of low-frequency, quasi-localized modes[23] and a decrease in the local variation of the elasticity[51]. We hypothesize that these two features are the cause of the differences in the low-frequency energy transport.

More work is needed in order to understand energy transport beyond the harmonic approximation. Two level tunneling states are postulated to describe many aspects of the universal low temperature properties of amorphous solids[3,5,7]. Since these states arise from two nearby energy minima due to small rearrangements of particles, it may be possible to identify the classical analogues of these states in classical model glassy systems. This would allow for a more detailed investigation of the low temperature thermal conductivity. Recent studies indicate that the finite temperature sound attenuation is modified[52,53], and thus the thermal diffusivity would be expected to change. To examine these changes in the energy transport one could study wave packets running molecular dynamics simulations with the full potential instead of the harmonic approximation used here.

Conflicts of interest

There are no conflicts to declare.

8 Acknowledgements

We gratefully acknowledge the support of NSF Grants DMR-1608086 (E.F., L.W. and G.S) and CHE-1800282 (E.F. and G.S.), and the Start-up Fund from Anhui University through Grant S020318001/02 (L.W.).

Notes and references

1 A. Eucken, *Ann. Phys. (Leipzig)*, 1911, **34**, 185.
2 C. Kittel, *Phys. Rev.*, 1949, **75**, 972-974.
3 R. C. Zeller and R. O. Pohl, *Phys. Rev. B*, 1971, **4**, 2029-2041.
4 M. P. Zaitlin and A. C. Anderson, *Phys. Rev. B*, 1975, **12**, 4475-4486.
5 P. W. Anderson, B. I. Halperin and C. M. Varma, *Philos. Mag.*, 1972, **25**, 1-9.
6 W. A. Phillips, *J. Low Temp. Phys.*, 1972, **7**, 351-360.
7 R. O. Pohl, X. Liu and E. Thompson, *Rev. Mod. Phys.*, 2002, **74**, 991-1013.
8 R. B. Stephens, *Phys. Rev. B*, 1973, **8**, 2896-2905.
9 V. Lubchenko and P.G. Wolynes, *Phys. Rev. Lett.*, 2001, **87**, 195901.
10 V. Lubchenko and P. G. Wolynes, *Proc. Natl. Acad. Sci. USA*, 2003, **100** 1515-1518.
11 V. Lubchenko, *Adv. Phys.: X*, 2018, **3**, 1510296.
12 A. J. Leggett and D. C. Vural, *J. Phys. Chem. B*, 2013, **117**, 12966-12971.
13 C. C. Yu, *J. Non-Cryst. Solids*, 1991, **131**, 310-312.
14 J. C. Burton and S. R. Nagel, *Phys. Rev. E*, 2016, **93**, 032905.
15 P. B. Allen and J. L. Feldman, *Phy. Rev. Lett.*, 1989, **62**, 645-648.
16 P. B. Allen and J. L. Feldman, *Phys. Rev. B*, 1993, **48**, 12581-12588.
17 N. Xu, V. Vitelli, M. Wyart, A. J. Liu and S. R. Nagel, *Phys. Rev. Lett.*, 2009, **102**, 038001.
18 V. Vitelli, N. Xu, M. Wyart, A. J. Liu and S. R. Nagel, *Phys. Rev. E*, 2010, **81**, 021301.
19 U. Buchenau, Y. M. Galperin, V. L. Gurevich, D. A. Parshin, M. A. Ramos and H. R. Schober, *Phys. Rev. B*, 1992, **46**, 2798-2808.
20 D. A. Parshin, *Phys. Rev. B*, 1994, **49**, 9400-9418.
21 P. Debye, *Ann. Phys.*, 1912, **34**, 789.
22 E. Lerner, G. Düring and E. Bouchbinder, *Phys. Rev. Lett.*, 2016, **117**, 035501.
23 L. Wang, A. Ninarello, P. Guan, L. Berthier, G. Szamel and E. Flenner, *Nat. Commun.*, 2019, **10**, 26.
24 H. Mizuno and A. Ikeda, *Phys. Rev. E*, 2018, **98**, 062612.
25 J. L. Feldman, M. D. Kluge, P. B. Allen, F. Wooten, *Phys. Rev. B*, 1993, **48**, 12589-12602.
26 W. Schirmacher, *Europhys. Lett.*, 2006, **73**, 892-898.
27 D. G. Cahill and R. O. Pohl, *Solid State Commun.*, 1979, **70**, 927-930.

28 Y. M. Beltukov, D. A. Parshin, V. M. Giordano and A. Tanguy, *Phys. Rev. E*, 2018, **98**, 023005.

29 C. Kittel, *Introduction to Solid State Physics*, John Wiley and Sons, New York, 1996.

30 Y. M. Beltukov, C. Fusco, D. A. Parshin, and A. Tanguy, *Phys. Rev. E*, 2016, **93**, 023006.

31 P. Sheng and M. Zhou, *Science*, 1991, **253**, 539-542.

32 P. B. Allen, J. L. Feldman, J. Fabian and F. Wooten, *Phil. Mag B*, 1999, **97**, 1715-1731.

33 L. Wang, L. Berthier, E. Flenner, P. Guan and G. Szamel, *Soft Matter*, 2019, **15**, 7018-7025.

34 A. Moriel, G. Kapteijns, C. Rainone, J. Zylberg, E. Lerner and E. Bouchbinder, *J. Chem. Phys.*, 2019, **151**, 104503.

35 E. Bitzek, P. Koskinen, F. Gähler, M. Moseler and P. Gumbsch, *Phys. Rev. Lett.*, 2006, **97**, 170201.

36 L. Berthier, D. Coslovich, A. Ninarello and M. Ozawa, *Phys. Rev. Lett.*, 2016, **116**, 238002.

37 A. Ninarello, L. Berthier and D. Coslovich, *Phys. Rev. X* , 2017, **7**, 021039.

38 E. Bouchbinder and E. Lerner, *New J. Phys.*, 2018, **20**, 073022.

39 S. John, H. Sompolinsky and M. J. Stephen, *Phys. Rev. B*, 1983, **27**, 5592-5603.

40 H. Mizuno, H. Shiba and A. Ikeda, *Proc. Natl. Acad. Sci. USA*, 2017, **114**, E9767-E9774.

41 E. Lerner and E. Bouchbinder, *Phys. Rev. E*, 2017, **96**, 0201104(R).

42 G. Kapteijns, E. Bouchbinder and E. Lerner, *Phys. Rev. Lett.*, 2018, **121**, 055501.

43 L. Angelani, M. Paoluzzi, G. Parisi and G. Ruocco, *Proc. Natl. Acad. Sci. USA*, 2018, **115**, 8700-8704.

44 U. Buchenau, Yu. M. Galperin, V. L. Gurevich and H. R. Schober, *Phys. Rev. B*, 1991, **43**, 5039-5045.

45 H. R. Schober and C. Oligschleger, *Phys. Rev. B*, 1996, **53**, 11469-11480.

46 V. L. Gurevich, D. A. Parshin and H. R. Schober, *Phys. Rev. B*, 2003, **67**, 094203.

47 W. Schirmacher, G. Ruocco and T. Scopigno, *Phys. Rev. Lett.*, 2007, **98**, 025501.

48 F. P. Benetti, G. Parisi, F. Pietracaprina and G. Sicuro, *Phys. Rev. E*, 2018, **97**, 062157.

49 E. M. Stanifer, P. K. Morse, A. A. Middleton and M. L. Manning, *Phys. Rev. E*, 2018, **98**, 042908.

50 H. Ikeda, *Phys. Rev. E*, 2019, **99**, 050901(R).

51 A. Shakerpoor, E. Flenner and G. Szamel, *arXiv:1909.12364*, 2019.

52 H. Mizuno, G. Ruocco and S. Mossa, *arXiv:1905.10235*, 2019.

53 H. Mizuno and S. Mossa, *arXiv:1906.08012*, 2019.